Smart Structures and Systems, *Vol. 30, No. 5 (2022) 463-477*
https://doi.org/10.12989/sss.2022.30.5.463

Hybrid vibration-impedance monitoring in prestressed concrete structure with local strand breakage

Ngoc-Loi Dang [1a], Quang-Quang Pham [2b] and Jeong-Tae Kim*[2]

[1] *Urban Infrastructure Faculty, Mien Tay Construction University, Vinh Long 890000, Vietnam*
[2] *Department of Ocean Engineering, Pukyong National University, Nam-gu, Busan 48513, Korea*

(*Received April 11, 2022, Revised August 19, 2022, Accepted August 22, 2022*)

Abstract. In this paper, a hybrid vibration-impedance-based damage monitoring approach is experimentally evaluated for prestressed concrete (PSC) structures with local strand breakage. Firstly, the hybrid monitoring scheme is designed to alert damage occurrence from changes in vibration characteristics and to localize strand breakage from changes in impedance signatures. Secondly, a full-scale PSC anchorage is experimented to measure global vibration responses and local impedance responses under a sequence of simulated strand-breakage events. Finally, the measured data are analyzed using the hybrid monitoring framework. The change of structural condition (i.e., damage extent) induced by the local strand breakage is estimated by changes in a few natural frequencies obtained from a few accelerometers in the structure. The damaged strand is locally identified by tomography analysis of impedance features measured via an array of PZT (lead-zirconate-titanate) sensors mounted on the anchorage. Experimental results demonstrate that the strand breakage in the PSC structure can be accurately assessed by using the combined vibration and impedance features.

Keywords: hybrid monitoring; impedance response; prestressed concrete structure; PZT interface; strand breakage; vibration response

1. Introduction

Prestressed concrete (PSC) has been extensively applied for the construction of bridges thanks to its advantages, such as better structural performance and diminution or exclusion of cracks. For post-tensioning structures, steel strands are prestressed and anchored into an anchorage zone. The anchorage zone plays a vital role in transferring prestressing force to the main structure. During construction, PSC structures often face instant prestress loss induced by elastic shortening of concrete elements and relative movement between the wedges-anchor head. Moreover, prestress-force levels could be dismissed due to time-dependent losses induced by corrosion and relaxation of prestressing strands as well as creep and shrinkage of concrete members (Tadros *et al*. 2003). The long-term monitoring of prestressing force shows that losses could reach 7.7% in seven years after being constructed (Hiba and Glisic 2018). Thus, it demands the development of effective structural health monitoring (SHM) techniques to properly monitor prestress-force and prevent tragic collapses of PSC structures in the future (Putcha *et al*. 2020).

Various SHM techniques have been developed to evaluate the health states of PSC structures (Lee and Kalos 2014, Hiba and Glisic 2019, Bonopera *et al*. 2020). In general, global SHM methods utilize changes in vibration characteristics to detect the integrity of an entire structure. Local SHM methods are commonly used to detect structural damage at local zones or critical connections (Ye *et al*. 2019, Yu *et al*. 2021). Meanwhile, combined global-local SHM methods could yield effective condition assessment because they can alarm global damage occurrence and quantify local damage characteristics.

By utilizing the global SHM concept, structural damage in a PSC beam was successfully identified using changes in modal frequencies and mode-shapes (Kim *et al*. 2003). Also, cable-force estimation in a cable-stayed structure was also achieved using the change in natural frequencies induced by the variation of cable stiffness (Zui *et al*. 1996, Fang and Wang 2010). Despite the research attempts, damage assessment in prestressed multi-strands has not been significantly conducted especially using experimental data so far.

During the last few decades, local SHM methods have also been recognized for PSC members by researcher communities. Abdullah *et al*. (2015a) utilized relative strain variations measured via electrical strain gages to localize damaged strands in a multi-strands anchorage. Also, strand-embedded fiber optic strain sensors were proposed for prestress-force estimation in PSC bridges (Lan *et al*. 2014). Meanwhile, electromechanical impedance monitoring techniques have been recognized for monitoring PSC members (Nguyen and Kim 2012, Min *et al*. 2016, Ai *et al*. 2019, Dang *et al*. 2020b). A lead-zirconate-titanate (PZT) patch is mounted on an inspected structure to gain impedance responses under an applied harmonic voltage.

*Corresponding author, Ph.D., Professor,
E-mail: idis@pknu.ac.kr
[a] Ph.D.
[b] Post-Doctoral Researcher

ISSN: 1738-1584 (Print), 1738-1991 (Online)

Impedance features (e.g., peak frequencies or statistical damage metrics) are then used to assess structural damage. It is known that an anchorage system of a PSC structure is supported by a stiff steel-anchor block (Nie *et al*. 2014) or a concrete block (Nawy 2010, Cervenka and Ganz 2014). Although the impedance monitoring techniques have been successfully implemented to the anchorage system for estimating changes in prestress-force (Min *et al*. 2016, Dang *et al*. 2020b), intensive experimental studies on multi-strands concrete anchorage are still needed to identify the local breakage of strands.

As hybrid SHM approaches, multiple techniques using features of modal frequency, acoustic emission, and DIC (digital image correlation) have been developed for damage evaluation in concrete structures (Lacidogna *et al*. 2019, 2020). Moreover, the hybrid vibration-impedance approach has been developed to detect concrete damage and prestress loss in a mono-strand girder bridge (Kim *et al*. 2010). So far, most previous studies have applied hybrid SHM techniques for reinforced concrete structures or a lab-scaled mono-strand PSC structure to detect structural damage. For multi-strand PSC structures (e.g., an anchorage zone), a local strand breakage is defined as the damage at a strand in forms of prestress-loss or fracture. In prestressed concrete structures, the local strand breakage should be monitored to appropriately assess the integrity of the whole structure. Thus, the hybrid vibration-impedance approach should be practically applied to deal with strand-breakage detection in two ways. First, the vibration-based monitoring provides global estimations of structural conditions (e.g., damage occurrence and damage extent). Second, the impedance-based monitoring produces pin-point localization of damage and detection of damage in the forms of physical behaviors. First, the vibration-based monitoring provides global estimations of structural conditions (e.g., damage occurrence and damage extent). Second, the impedance-based monitoring produces pin-point localization of damage and detection of damage in the forms of physical behaviors. Third, the hybrid approach enables online and real-time monitoring capability (Abdulkarem *et al*. 2019, Hoang *et al*. 2020).

In this study, a hybrid vibration-impedance-based damage monitoring approach is experimentally evaluated for prestressed concrete (PSC) structures with local strand breakage. The hybrid monitoring scheme is designed to alert damage occurrence from changes in vibration characteristics and to localize strand breakage from changes in impedance signatures. A full-scale PSC anchorage is experimented to measure global vibration responses and local impedance responses under a sequence of simulated strand-breakage events. Then, experimental results are analyzed to evaluate the proposed hybrid monitoring framework.

2. Hybrid monitoring framework for strand-breakage detection in PSC structure

2.1 Design of hybrid monitoring framework

The loss of prestress force below an assured threshold could result in severe damage to a PSC structure. A hybrid vibration-impedance-based damage monitoring in a PSC structure with local strand breakage is illustrated as shown in Fig. 1. The PSC girder is designed with multiple tendons and anchorages. As shown in Fig. 1(a), prestressed multi-strands are anchored to keep control of prestressed forces and transfer them into the girder. A few accelerometers are mounted to measure vibration data (i.e., global responses) of the PSC structure. PZT interfaces are installed on anchorages to measure impedance data (i.e., local responses) of the local anchorage zones.

As shown in Fig. 1(b), the strand breakage causes changes in acceleration features of the entire structure and impedance signatures of the local PZT sensing zone. Therefore, the strand-breakage event in the PSC structure can be identified from inverse analyses of vibration responses and impedance responses. The change in global structural conditions induced by the local strand breakage is estimated from the change in modal frequencies extracted from acceleration features. The change in the local anchorage zone is detected directly from the change in

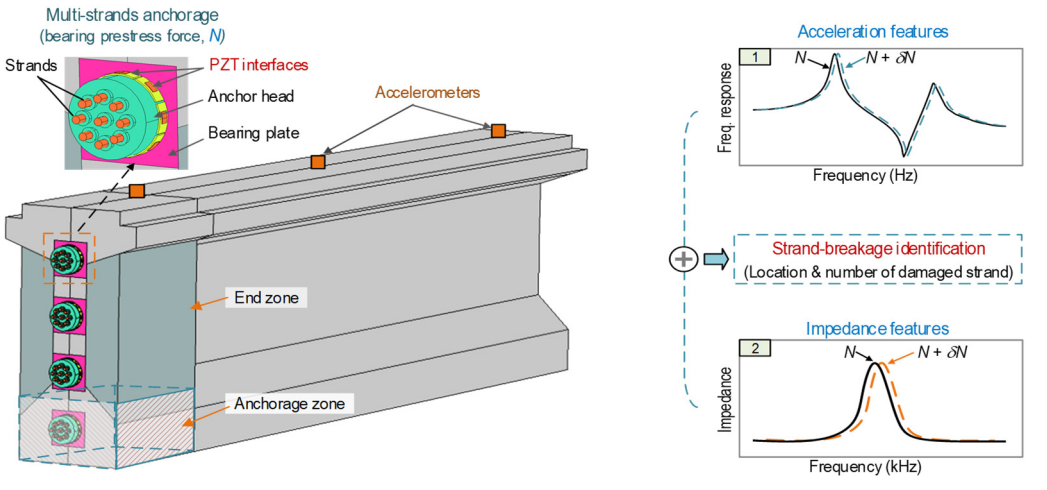

(a) PSC girder with multiple tendons (b) Global-local structural responses

Fig. 1 Hybrid vibration-impedance monitoring concept for PSC structure

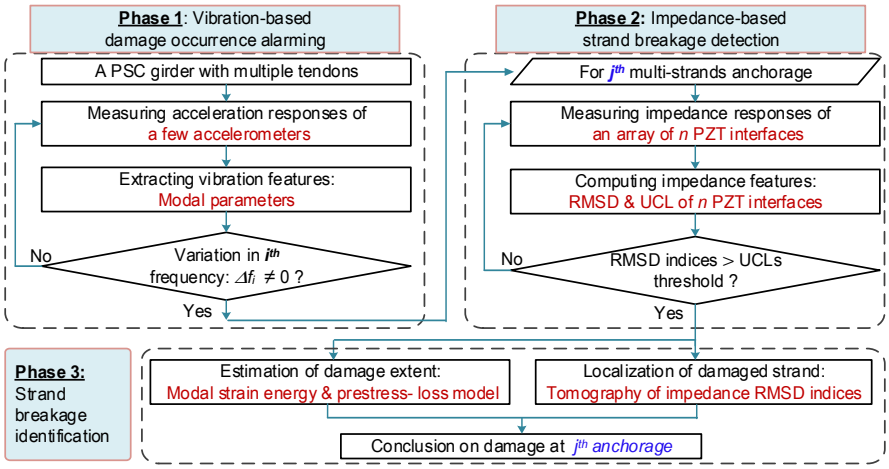

Fig. 2 Schematic vibration and impedance-based damage monitoring in PSC structure

impedance features sensed from PZT interfaces.

Based on the concept of hybrid vibration-impedance monitoring techniques for damage detection in a PSC beam (Kim *et al*. 2010), the strand-breakage monitoring framework is designed with three phases (Phases 1-3), as shown in Fig. 2. Phase 1 is vibration-based damage occurrence alarming. Once prestress-loss occurs in any strands, it could yield variations of modal parameters of the whole structure. Then, the change of global structural conditions induced by prestress-loss can be determined by measuring changes in modal frequencies. Phase 2 is impedance-based strand breakage detection. Once the damage existence is alerted, the impedance-based strand breakage detection is activated. Measured impedance features of the PZT interface array are used to determine whether damage occurrence at the anchorage.

Phase 3 is strand breakage identification. When the strand breakage event occurs at the anchorage, the strand breakage identification is triggered. The damage extent is estimated based on changes in modal frequency. The vibration-based monitoring estimates the reduction of modal strain energy and the prestress loss from which the extent of failed strands can be predicted with respect to the intact strands. Locations of potentially damaged strands are identified by using tomography analysis of RMSD (root-mean-square-deviation) indices. The combination of vibration-impedance features suggests the final decision on damaged strands.

2.2 Vibration-based damage occurrence alarming

2.2.1 Output-only modal analysis

Dynamic motions of a PSC structure under ambient vibration can be defined as follows

$$\ddot{v}_t = (P_t - [C]\dot{v}_t - [K]v_t)[M]^{-1} \quad (1)$$

where [M], [C], and [K], are matrices of mass, damping, and stiffness; P_t is a vector of excitation force, and $\ddot{v}_t$, $\dot{v}_t$, and v_t and are vectors of the acceleration, velocity, and displacement responses, respectively.

The acceleration responses represent dynamic behaviors of the investigated structure subjected to excitation forces. In practice, the excitation P_t is very hard to implement, so that output-only acceleration signals can be measured under ambient excitation sources (e.g., traffic or wind loads). Then the frequency-domain decomposition (FDD) analysis is commonly employed to extract modal parameters such as natural frequencies and mode shapes from the output-only vibration information (Brincker *et al*. 2001, Yi and Yun 2004, Park 2009).

In the FDD method, output-only acceleration signals are used to determine modal parameters of the inspected structure. At first, a set of structural responses are measured via n accelerometers. Then, a matrix $S_{yy}(\omega)$ of power spectral density is calculated using the n output responses. The matrix $S_{yy}(\omega)$ is again decomposed into unitary matrices $U(\omega)$ and $V(\omega)$ and a diagonal matrix $\sum(\omega)$, as follows

$$S_{yy}(\omega) = U(\omega)^T \sum(\omega) V(\omega) \quad (2)$$

Lastly, a peak frequency can be found in $\sigma_l(\omega)$, and the mode shape corresponding to the frequency is determined from any one of a column of $U(\omega)$.

2.2.2 Strand-breakage assessment using vibration features

Structural damage leads to the change in modal parameters, thus enabling the use of modal parameters for global damage detection (Kim *et al*. 2003, Cho *et al*. 2009, Lee *et al*. 2018). Since natural frequencies can be extracted from just a few measured locations and are less prone to noise (e.g., ambient vibrations) (Wei and Pizhong 2010), it is commonly used for alarming damage occurrence in an inspected structure. Meanwhile, mode shapes should be identified to characterize vibrational modes of natural frequencies.

This study utilizes changes in natural frequencies as a damage indicator for alarming global damage existence in a PSC structure (Richmond *et al*. 2020). The change of structural condition induced by the strand-breakage event is estimated by the variation of modal strain energy that can be approximately computed using modal parameters.

Fractional changes in modal strain energies are estimated by relative changes in natural frequencies (Gudmundson 1982, Kim and Stubbs 2003), as follows

$$\left(\frac{\delta W}{W}\right)_i \approx \frac{\delta\omega_i^2}{\omega_i^2} \tag{3}$$

where W_i and δW_i are the i^{th} modal strain energy of the pristine structure and its loss after damage. The terms ω_i and $\delta\omega_i$ are the i^{th} natural frequency of the pristine state and its relative change after structural damage.

In the study, the feasibility of the hybrid vibration-impedance monitoring is experimentally evaluated on a real-scaled anchorage of the PSC structure. The test structure is intently designed as a symmetric structure with a centrally prestressed tendon (a tendon with 9-strands). Moreover, the PSC structure was assumed as a beam model, so the loss of prestress force can be estimated using prestress-loss model proposed by Kim *et al*. (2004).

For a beam model with a centrally prestressed tendon, the prestress loss (δN) can be estimated with respect to the full prestress force (N_f) by utilizing relative changes in modal frequencies ($\delta\omega_i$), as follows

$$\left(\frac{\delta N}{N_f}\right)_i = \frac{\delta\omega_i^2}{\omega_{f,i}^2 - \omega_{o,i}^2} \tag{4}$$

where $\omega_{f,i}$ and $\omega_{o,i}$ are i^{th} natural frequencies measured at the full prestress force (N_f) and zero prestress force, respectively. As seen in Eq. (4), the accuracy of the force-loss prediction depends on the i^{th} measured natural frequency of a structure.

To enable the performance of strand breakages of a PSC structure, a multi-strand anchorage zone was installed on the stressing frame (i.e., supporting structure). The tested structure was designed as a centrally prestressed structure, and it was assumed as a beam model. As a beam structure, the prestress-loss model (Kim *et al*. 2004) is adopted for predicting force-loss in the structure.

2.3 Impedance-based strand-breakage detection

2.3.1 Hoop-type PZT interface for PSC anchorage

Based on the concept of the PZT interface technique for impedance monitoring (Huynh and Kim 2014), a hoop-type PZT interface for local dynamic monitoring of a PSC anchorage system is proposed, as shown in Fig. 3. Each prestressed strand is clamped into a conical hole of the circular anchor head with a friction surface of slope angle α, as shown in Fig. 3(a). A prestress force F_P causes a friction force F_W at the interface of wedge-anchor head and a radial force F_R in the anchor head. On the circumference of the anchor head, local hoop stress σ_θ and axial stress σ_z are caused by the forces F_R and F_P. Due to the bending nature of the anchorage under the force F_P, the near-bottom anchor head experiences axial-compressive stress and hoop-tensile stress.

As shown in Fig. 3(b), a hoop-type PZT interface is designed for the circular anchorage to measure impedance signatures from coupling interactions between the PZT interface and the anchor head (Dang *et al*. 2020b). The PZT interface is designed with two affixed parts and a flexible part. The flexible part equipped with a PZT sensor is considered to enhance PZT's impedance signals, and the affixed parts interact with the mechanical anchor head. It is assumed that steel strands are prestressed before the PZT interfaces are implemented to monitor the health state of prestressing strands. Once a prestressing strand is damaged (e.g., Strand 4 damaged), stress-field changes locally occur

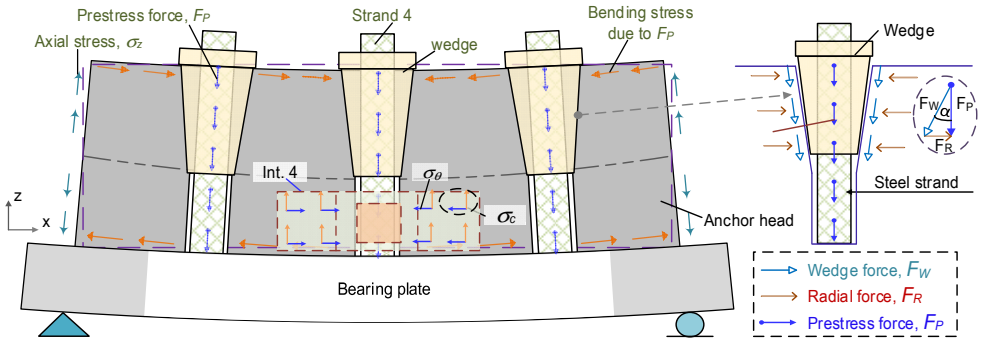

(a) Circular anchor head, bearing plate, and PZT interface under prestress-force

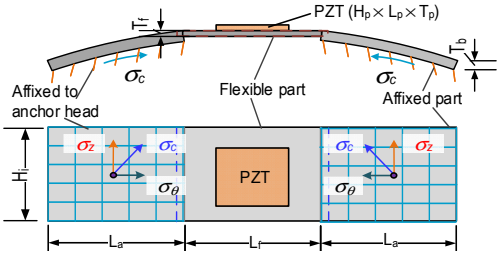

(b) Hoop-type PZT interface under stress variation

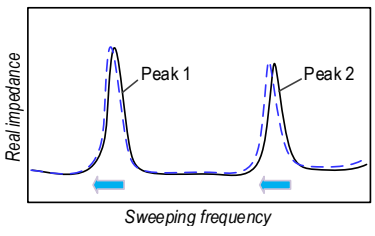

(c) Shifts of PZT interface's natural frequencies

Fig. 3 Hoop-type PZT interface for local dynamic monitoring of PSC anchorage system

in the anchor surface.

From the related works (Abdullah *et al*. 2015a, Dang *et al*. 2020a), it is expected that stress variations occur significantly at the bottom of the anchor head. Since the PZT interface (i.e., Int. 4 in Fig. 3(a)) is affixed to the anchor head, its flexible part (see Fig. 3(b) is along with the axial stress σ_z and the hoop stress σ_θ of the anchor head (Dang *et al*. 2020a). Therefore, dynamic properties of the PZT interface vary dependent on the variation of the compressive stress σ_c applied to the interface. By treating the PZT interface as a fixed-fixed beam under an axial compressive force, its dynamic characteristics (e.g., natural frequencies) can be estimated as follows (Clough and Penzien 1995, Dang *et al*. 2020b)

$$\omega_m = \frac{C_m}{2}\sqrt{1-\frac{4PL_f^2}{\pi^2 EI}\frac{C_1}{C_m}}\sqrt{\frac{EI}{mL_f^4}} \tag{5}$$

where C_1 and C_m are constant coefficients determined from a fixed-type beam for the 1^{st} and m^{th} modes (Clough and Penzien 1995); P is a force caused by the compressive stress σ_c, and L_f and EI are the length and flexural rigidity of the interface.

As observed in Eq. (5), the variation of the force P would change the natural frequencies (see Fig. 3(c)). Inversely, the variation of resonant frequencies measured from the PZT interface can be utilized to estimate the change of the axial force applied to the interface, indicating the change in prestress-force of the anchorage nearby the PZT sensor.

2.3.2 Two-DOFs impedance model for hoop-type PZT interface

As shown in Fig. 4, the interaction between the PZT interface and the inspected structure can be simplified as a 2-DOFs impedance model (Huynh and Kim 2017). One DOF stands for the motion of the PZT interface, and the other represents the motion of the inspected structure. The coupled structural-mechanical (SM) impedance, $\overline{Z}(\omega)$ of the interface-anchorage at the PZT-driven point can be written

$$\bar{Z}(\omega) = \frac{K_{11}(\omega)K_{22}(\omega) - K_{12}^2(\omega)}{i\omega K_{22}(\omega)} \tag{6}$$

where dynamic stiffness coefficients are derived as $K_{11} = -\omega^2 m_i + i\omega c_i + k_i$, $K_{12} = -i\omega c_i - k_i$, and $K_{22} = -\omega^2 m_s + i\omega(c_i+c_s) + (k_i+k_s)$.

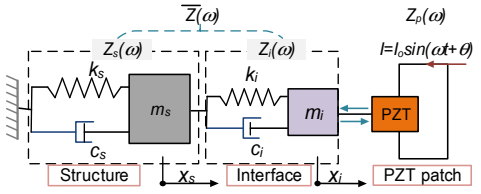

Fig. 4 Two DOF impedance model of an inspected structure-PZT interface

The terms m_s, c_s, k_s and m_i, c_i, k_i are the masses, damping coefficients, and spring stiffness of the inspected structure and the interface, respectively. The stiffness coefficients depend on the structural parameters of the inspected structure and interface.

The SM impedance of the PZT patch, $Z_p(\omega)$ and the one of interface-inspected structure, $Z_s(\omega)$ are coupled together (Liang *et al*. 1994)

$$Z(\omega) = \left\{ i\omega A\left[\hat{\varepsilon}_{33}^T - \frac{1}{Z_p(\omega)/\bar{Z}(\omega)+1} d_{31}^2 \hat{Y}_{11}^E\right]\right\}^{-1} \tag{7}$$

where A, $\hat{Y}_{11}^E$, d_{31}, and $\hat{\varepsilon}_{33}^T$ are geometric constants of the PZT patch, the complex Young's modulus patch at zero electric fields, the piezoelectric coupling constant, and the complex dielectric constant zero stress, respectively. Once the PZT patch has no changes in mechanical properties or electrical characteristics and no energy loss induced by contact conditions between the interface-anchorage, the SM impedance $Z_p(\omega)$ remains constant. Thus, any changes in the monitored structure (e.g., a damaged strand) that cause shifts in impedance frequencies can be measured via the interface technique.

The change of prestress force yields the variation of impedance response (Yang *et al*. 2008a, Dang *et al*. 2019). For a multi-strand anchorage, the sensitivity of a PZT's impedance response is dependent on its relative position to damaged strands. For multiple PZT sensors on an anchorage, RMSD (root-mean-square-deviation) magnitudes of their impedance responses can be quantified to localize the damaged strands on the anchorage.

The RMSD damage metric is estimated to quantify changes in impedance signals (Giurgiutiu and Rogers 1998)

$$RMSD(Z,Z^*) = \sqrt{\left(\sum_{i=1}^{N}[Z^*(\omega_i)-Z(\omega_i)]^2\right)\Big/\sum_{i=1}^{N}[Z(\omega_i)]^2} \tag{8}$$

where $Z(\omega_i)$ and $Z^*(\omega_i)$ are impedance signatures obtained from the pristine state and a later state (i.e., a damaged state) of the structure at the i^{th} frequency, and N is the total frequency points. A RMSD magnitude (which is calculated by averaging test ensembles) is zero for the pristine state. A control threshold is used to make a decision on damage existence as follows

$$UCL = \mu + 3\sigma \tag{9}$$

where the mean value μ and standard deviation σ are calculated from at least four ensembles of impedance signatures measured at the pristine state. When the RMSD magnitude of impedance signals at a later state is larger than the control threshold, it indicates the damaged state with the 99.7% confidence level.

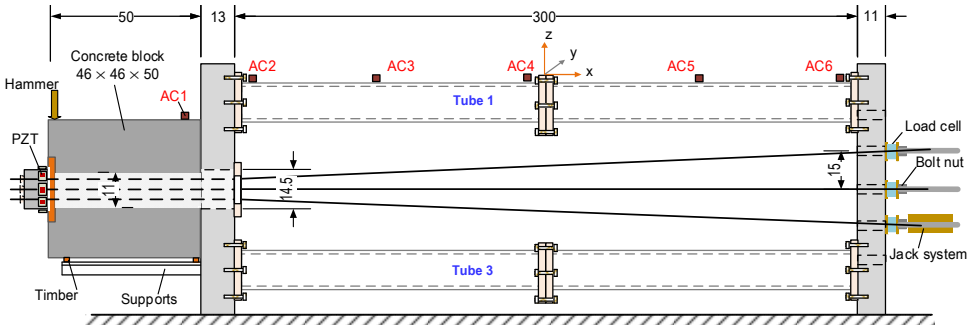

(a) Sketch up of anchorage zone on the testing frame

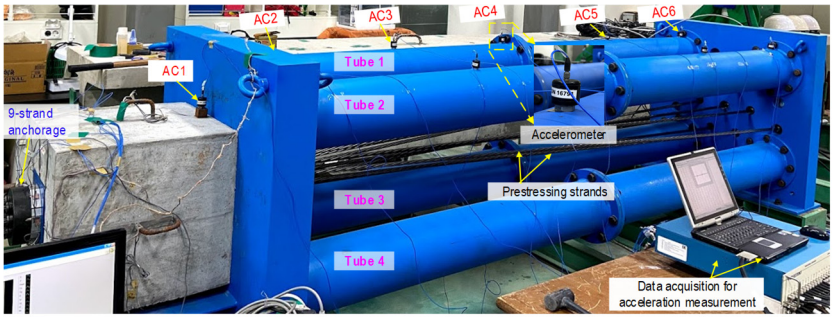

(b) Real view of accelerometer deployment on test structure

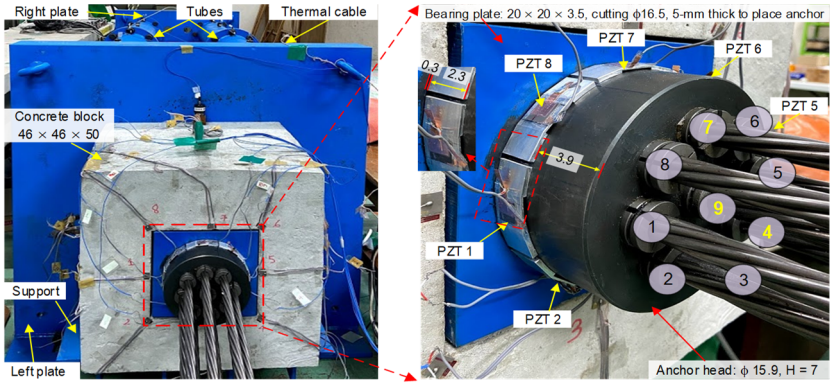

(c) Test setup of anchorage zone (d) PZT interfaces on anchor head

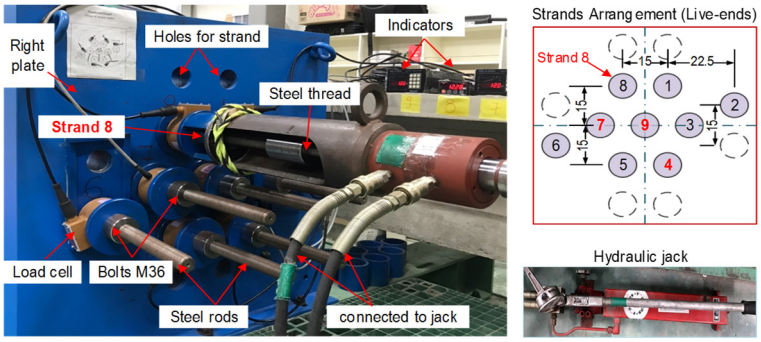

(e) Detailed setup of right-end strands

Fig. 5 Experimental setup in anchorage zone and testing frame (dimension in cm)

3. Vibration-impedance tests on PSC structure with strand-breakage

3.1 Test structure and sensor deployment

3.1.1 Overview of test setup

The hybrid vibration-impedance monitoring framework was experimentally evaluated on a lab-scale PSC structure. Fig. 5 shows the experimental setup of a multi-strands anchorage zone on a testing frame. The frame represented the remaining part of a PSC structure. The test structure with the loading capacity of 3000 kN was intently designed to resist prestressing forces.

Experimental setups were made in four steps. First, a

concrete anchorage with a proper design of reinforcement was fabricated and cured in laboratory conditions. Second, the concrete anchorage (casting after 21-day) with an anchor head, a bearing plate, and nine steel strands were installed into the testing frame to form a post-tensioned anchorage zone with unbonded cables. Third, the anchorage zone was gradually prestressed up to 1059.5 kN by nine strands. Lastly, measurement systems were setup to measure vibration-impedance responses under simulated strand breakage events. All experimental works were conducted under near-constant temperature at Smart Structure engineering Laboratory, Pukyong National University, Korea.

3.1.2 Description of test structure

The design of the anchorage zone was selected based on the recommendation of VSL International Ltd. (VSL 2018). Passage tubes (ϕ 11 cm, l = 46.5 cm) were placed at the center of the concrete block to form unbonded cables. The anchorage zone consists of a concrete block (46 × 46 × 50 cm), an anchor head (ϕ 15.9 cm and 7 cm in height) for nine strands, and a bearing plate (20 × 20 × 3.5 cm). The concrete block was designed to resist a minimum compressive force of 1080 kN (120 kN per strand) by reinforcing orthogonal, spiral, and framed re-bars. The concrete had compressive strength f'_c = 23.3 MPa at 28 days (tested on a cylindrical sample with ϕ 15 cm and 30-cm thick). The 7-wire steel-strand (Grade 270 low relaxation steel) had 6.0 m in length and ϕ 15.2 mm. The material properties of the anchorage components were listed in Table 1.

As schematized in Fig. 5(a), the anchorage zone was positioned on the left side of the steel frame, which consists of two rigid steel plates and four tubular beams (each tube has ϕ_{inner} = 19.5 cm and ϕ_{outer} = 21.6 cm). On the dead end, prestressing strands were gripped into the anchor head using conical wedges before passing through two holes on the concrete block and the bearing plate. As shown in Fig. 5(a), a spacer plate was used to ensure prestressing strands that were placed at the center of the concrete block. Also, timber supports were used to ensure no eccentricity between the concrete block and the testing frame. As seen in Fig. 5(c), the right-end strands designed with steel rods were passed multiple circular holes (15 cm in the distance) on the rigid steel plate. The steel rod was connected to the steel thread of a hydraulic jack. Hydraulic jacks (Tonner jacking system with a capacity of 260 kN) were used to introduce the prestress force into the strand, and the force was maintained

Table 1 Material properties of anchorage components, PZT interface, and adhesive layer

Parameters	Steel anchorage	Concrete	Steel strand	PZT 5A patch	Aluminum interface	Loctite adhesive
Young's modulus E, (GPa)	200	24.4	197	62.1	70	5.0
Poisson's ratio ν	0.30	0.20	0.33	0.35	0.35	0.38
Mass density ρ (kg/m^3)	7850	2400	7850	7750	2700	1700
Compressive strength (MPa)	520	23.3	-	-	-	
Tensile strength (MPa)	460	2.3	1860	-	110	13.1

Table 2 Simulation of prestress force in test structure

Task	Case	Prestressing scenario								
Stressing cases	**SC-1**	About 0 kN for all strands								
	SC-2	353.2 kN for all of 9 strands from S1-S9(*)								
	SC-3	706.3 kN for all of 9 strands								
	SC-4	1059.5 kN for all of 9 strands								
Force adjustment		Strands 1, 3, 5-6, and 8 were adjusted (**)								
Strand breakage cases		Strand 1	Strand 2	Strand 3	Strand 4	Strand 5	Strand 6	Strand 7	Strand 8	Strand 9
	PS-1 (Intact)	118.7	119.2	118.7	117.7	119.2	118.4	116.7	118.7	118.7
	PS-2 (Strand 4)	118.9	119.9	119.7	0.0	121.4	119.3	117.7	119.7	119.7
	PS-3 (Strands 4&7)	119.7	120.1	120.2	1.0	122.4	120.2	1.0	120.3	120.7
	PS-4 (Strands 4,7,9)	120.5	120.9	120.7	1.7	122.9	121.1	1.5	121.2	0.0
	PS-5	About 0 kN for all strands(***)								

(*) Stressing sequence for SC1-SC4: Strand 9, Strands 1&5, Strands 3&7, Strands 4&8 tested on 1/11/2019.
(**) Prestress-force losses were about 0.82 % for 110 days after the first stressing performed on 2/18/2020.
(***) Sequence for PS-5: Strands 3&8, Strands 1&5, Strands 2&6. PS1~PS5 was tested on 2/20/2020

using bolts M36. Load cells were installed on all strands at the right end to control the applied forces.

To balance the test structure, each of the nine strands was prestressed by a small force of about 20 kN. All indicators of load cells were adjusted to zero (SC-1), and this state of test structure was set as the initial condition (so-called zero prestress-force). Nine strands were prestressed from zero (SC-1) to 1059.5 kN (SC-4) with three intervals (about 353 kN for each increment). During the prestress loading, a symmetric pair of cables (see Fig. 5(d)) was tensioned at the same time to keep the balance of structure. The loading sequence was Strand 9, Strands 1&5, Strands 3&7, Strands 2&6, and Strands 4&8. During a serious of jack-ups, prestress-forces of a few strands were adjusted to calibrate the change in prestress-forces of the strands, as noted in Table 2. Laboratory temperature was kept near 16°C using air-conditioners to minimize ambient effects on vibration and impedance signals.

3.1.3 Deployment of accelerometers and PZT interfaces

To measure vibration responses, one accelerometer (AC1) was placed on the concrete block, and five accelerometers (AC2-AC6) were mounted on the tubular beam (Tube 1) with an interval of 73.5 cm, as shown in Fig. 5(a). A rubber hammer excited the impulse to the top of the concrete block to acquire dynamic responses the six accelerometers (PCB 393B04 with a sensitivity of 1 V/g), as shown in Fig. 5(b). The measurement system includes a controller PXI-8186, data acquisition PXI-4472 of 16 channels, and a laptop with soft computing for the measurement process.

Eight hoop-type PZT interfaces (PZTs 1-8 matching to Strands 1-9) were positioned at the near-bottom anchorage (about 3.9 cm from the top of the anchor head) to acquire impedance responses, as shown in Figs. 5(c)-(d). Design parameters of the PZT sensor and the interface body (as referenced in Fig. 3(b)) were selected as follows: $H_p \times L_p \times T_p = 15 \times 15 \times 0.51$ mm for the PZT sensor, $H_i \times L_a \times T_a = 23 \times 18 \times 3.5$ mm for two affixed sections, and $H_i \times L_f \times T_f = 23 \times 24 \times 1.4$ mm for the flexible section. The material properties of the PZT interfaces, such as PZT 5A, aluminum interface, and Loctite adhesive, are listed in Table 1. PZT 5A patches were selected to acquire impedance responses. Loctite 401 (a high-strength instant adhesive) was used to attach PZT patches to aluminum interfaces and the interfaces to the anchor head.

3.2 Simulation of strand-breakage cases

Acceleration and impedance responses were sequentially measured for five test cases (PS-1~PS-5) outlined in Table 2. In PS-1 (the intact state), each of the 9 strands was prestressed up to about 118.5 kN. In PS-2, the breakage of Strand 4 was simulated by eliminating Strand 4's tension force while all other strands were kept at about 119.5 kN. In PS-3, the breakage of Strands 4 and 7 was simulated by eliminating Strands 4 and 7's forces while keeping the tension forces of other strands at about 120.8 kN. In PS-4, the breakage of Strands 4, 7, and 9 was simulated by eliminating those strands' forces while keeping the tension forces of other strands at about 121.7 kN. In PS-5, all strands were released to almost zero to simulate the last damage case.

Acceleration responses of the six accelerometers were recorded for a period of 30 seconds with sampling frequency f_s = 2 kHz. Four ensembles were recorded for each test case. Impedance responses of the eight PZT sensors were measured by applying 1V-harmonic excitation using HIOKI 3532 impedance analyzer. For the impedance tests, the frequency bandwidth was set as 5-35 kHz with 601 sweeping points. Four ensembles were recorded for each test case.

4. Hybrid vibration-impedance monitoring of strand breakage in PSC structure

4.1 Vibration-based damage estimation

4.1.1 Experimental modal analysis

As shown in Fig. 6, the acceleration signal was measured from AC4 on Tube 1 for the intact state (PS-1). For the first impact at 4.9 seconds, the maximum and

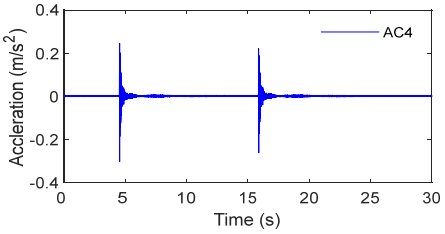

Fig. 6 Acceleration signals (AC4) on Tube 1 for intact case PS-1

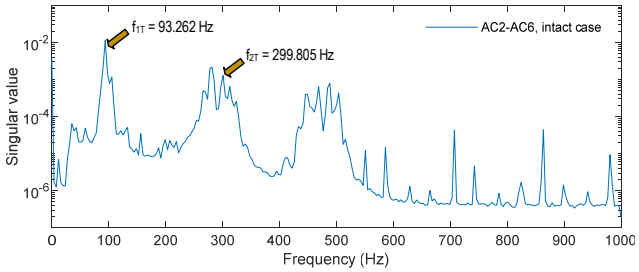

Fig. 7 Frequency-domain singular value analysis of acceleration signals for intact case PS-1

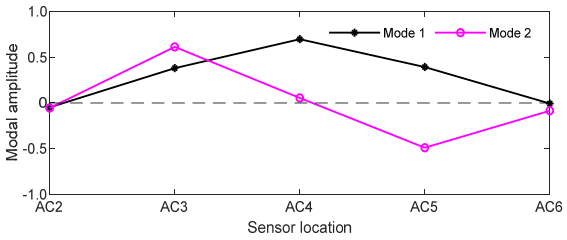

Fig. 8 Mode shapes extracted by FDD method using accelerometers AC2-AC6 for intact case PS-1

minimum magnitudes of AC4 were 0.25 m/s^2 and -0.30 m/s^2. To extract modal parameters of the test structure, the frequency resolution was selected as 0.4883 Hz corresponding to sampling frequency f_s = 2 kHz and a number of FFT $n_{FFT} = 2^{12}$. Modal parameters were extracted from the measured data in 30 seconds. The FDD method (see Eq. (2)) was utilized to determine the natural frequencies and corresponding mode shapes of the first two modes.

As shown in Fig. 7, frequency-domain singular value chart of acceleration signals (AC4) was plotted for the intact state (PS-1). The first and second resonant frequencies were extracted as f_1 = 93.262 Hz and f_2 = 299.805 Hz. It is noted that the tested structure was a composite structure, which included an anchorage zone with 9-strands, two supported plates, and Tubes 1-4. The measured acceleration signals could include in-plane (x-z axis in Fig. 5(a)) and out-of-plane vibrations of sub-structures, which lead to several small peaks close to 300 Hz. As shown in Fig. 8, two in-plane modes were extracted from sensors AC2-AC6. Hereafter, the two natural frequencies (f_1 = 93.262 Hz and f_2 = 299.805 Hz) were selected as the baseline to analyze the variation of vibration characteristics under strand breakage cases.

4.1.2 Variation of natural frequencies due to strand breakage

Table 3 shows the first two natural frequencies and their relative changes for the five test cases. Once the prestress force was totally lost (PS-5), the relative change of the 1st natural frequency (6.81%) was more significant than that of the 2nd peak (1.7%). The reduction of natural frequencies indicated the change in structural conditions induced by the strand breakage (Ho *et al*. 2012). As the loss of prestressing force was 117.7 kN due to the breakage of Strand 4, natural frequencies were reduced to 1.57% in mode 1 and 0.65% in mode 2. Due to the sequential losses induced by 235.4 kN (breakage of Strands 4&7) and 356.1 kN (breakage of Strands 4, 7&9), natural frequencies were reduced to 2.09~2.62% in mode 1 and 1.14~0.98% in mode 2. As noted in the table, the 2nd natural frequency was not extracted from AC2-AC6's signals (*N.A*, not available) for the test cases PS-2~PS-3. Moreover, the prestress losses in the anchorage zone can be reflected by changes in modal parameters of the test structure (i.e., Tube 1).

4.2 Impedance-based strand-breakage detection

4.2.1 PZT sensors' impedance signatures

As shown in Fig. 8, impedance responses of the intact state (PS-1) were measured from PZT1-PZT8 in the range of 5-35 kHz. Two clear resonant impedance peaks were observed for all PZT sensors: 9.5-11 kHz for Peak 1 (1.5 kHz bandwidth) and 25-28 kHz for Peak 2 (3.0 kHz bandwidth). The impedance signals measured via the PZT interface technique were well consistent, thus enabling the applicability of the technique for damage detection in practice.

As shown in Fig. 10, impedance responses for the breakage of Strand 4 (PS-2) were measured by PZT sensors (e.g., PZTs 2 and 4 in Fig. 10) in the frequency range of 5-35 kHz. Impedance signals of PZT 4 (close to the damaged Stand 4) shifted leftward while impedance signals of other sensors like PZT 2 remained almost unchanged. As shown

Table 3 Experimental natural frequencies of test structure under strand breakage cases

Case	Applied force (kN)		Natural frequency (Hz)				Frequency variation (%)			
	Total*	Losses	AC1 (Anchorage)		AC2-AC6 (Tube 1)		AC1 (Anchorage)		AC2-AC6 (Tube 1)	
			f_{1A}	f_{2A}	f_{1T}	f_{2T}	Δf_{1A}	Δf_{2A}	Δf_{1T}	Δf_{2T}
PS-1	1066.1	-	93.262	299.805	93.262	299.805	-	-	-	-
PS-2	956.3	117.7	91.797	297.852	91.797	*N.A*	-1.57	-0.65	-1.57	*N.A*
PS-3	845.4	235.4	91.309	296.387	91.309	*N.A*	-2.09	-1.14	-2.09	*N.A*
PS-4	730.3	356.1	90.820	296.875	89.844	296.875	-2.62	-0.98	-3.66	-0.98
PS-5	0	1066.1	86.914	294.922	86.914	294.434	-6.81	-1.63	-6.81	-1.79

*Total force was calculated by the sum of measured forces (see Table 2).

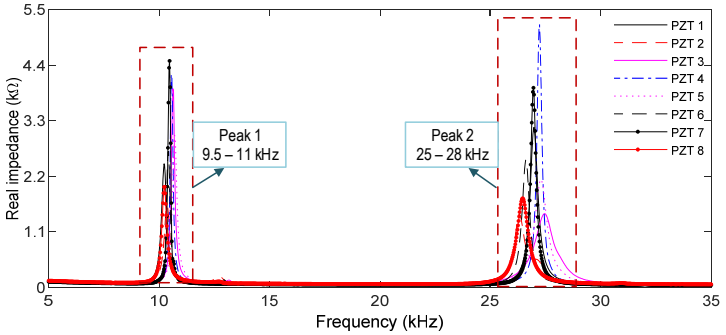

Fig. 9 Impedance responses of PZT1-PZT8 in the range 5-35 kHz for intact case (PS-1)

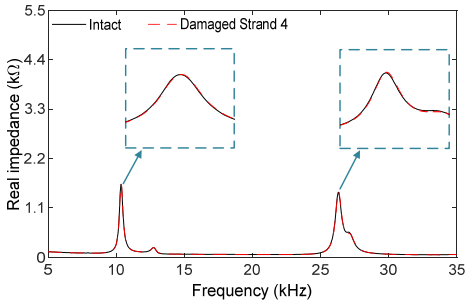

(a) PZT 2

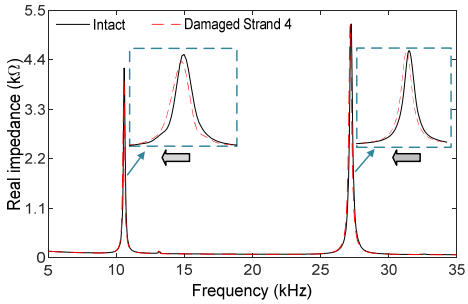

(b) PZT 4

Fig. 10 Impedance signals of PZT sensors for breakage of Strand 4 (PS-2)

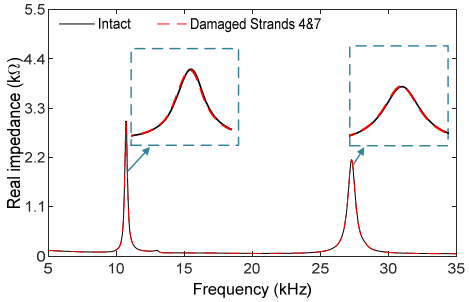

(a) PZT 5

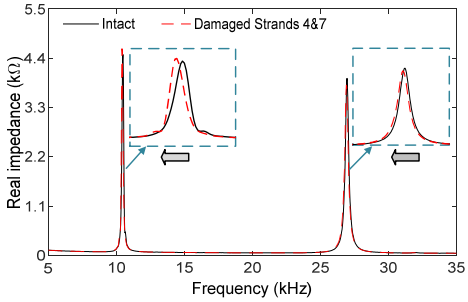

(b) PZT 7

Fig. 11 Impedance signals of PZT sensors under breakage of Strands 4&7 (PS-3)

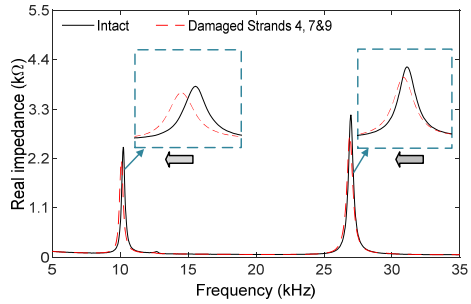

(a) PZT 1

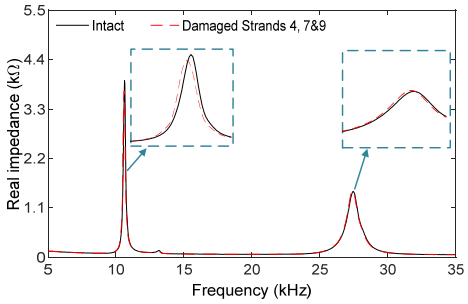

(b) PZT 3

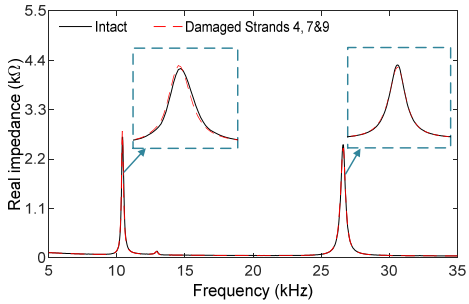

(a) PZT 6

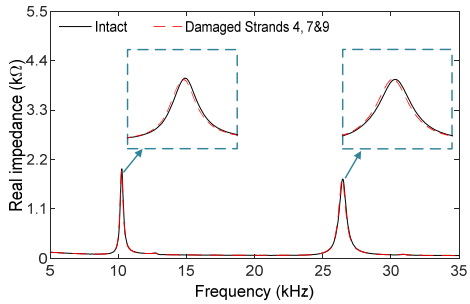

(b) PZT 8

Fig. 12 Impedance signals of PZT sensors under breakage of Strands 4, 7&9 (PS-4)

in Fig. 11, impedance responses for the breakage of Strands 4 and 7 (PS-3) were compared between PZT 5 (see Fig. 11(a)) and PZT 7 (see Fig. 11(b)). Impedance signals of PZT 7 (close to the damaged Strand 7) shifted leftward while impedance signals of other sensors had ignorable changes.

For the Strands 4, 7&9 breakage, Fig. 12 depicts impedance signatures of PZTs 1, 3, 6, and 8 in the measured frequency range. Noticing that all PZT sensors were placed the outer surface of the anchorage, those sensors were sensitive to the breakage of two outer strands (Strands 4 and 7) but less sensitive to the breakage of the center strand

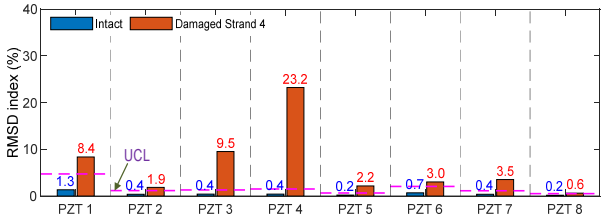

(a) Frequency range: 9.5-11 kHz (Peak 1)

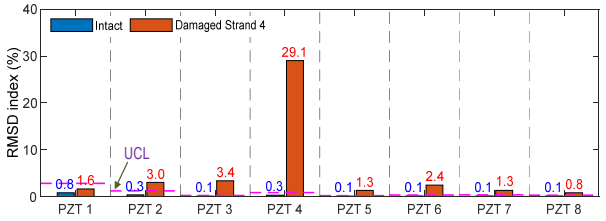

(b) Frequency range: 25-28 kHz (Peak 2)

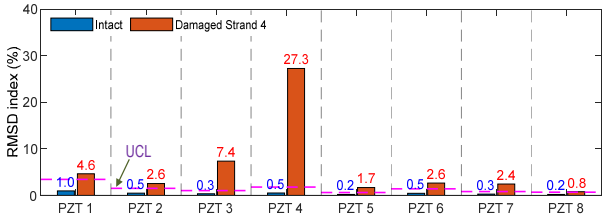

(c) Frequency range: 8-31 kHz

Fig. 13 RMSD indices of impedance responses under breakage of Strand 4

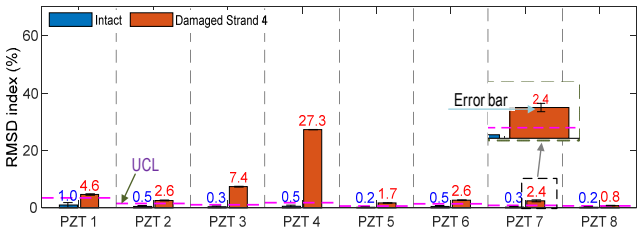

(a) Breakage of Strand 4

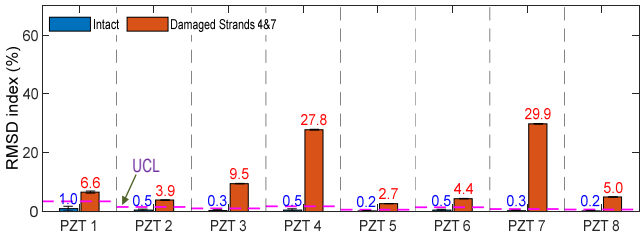

(b) Breakage of Strands 4&7

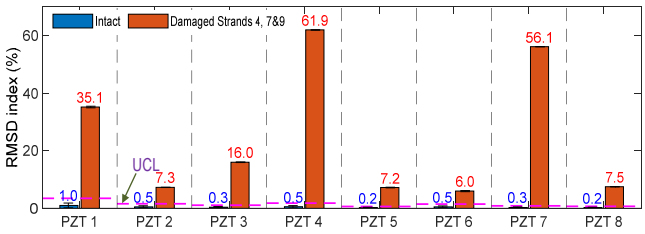

(c) Breakage of Strands 4, 7&9

Fig. 14 RMSD indices of impedance signatures calculated for frequency range 8-31 kHz

(Strand 9). Note also that all sensors had equal distances to the center strand (see Fig. 5(d)). The PZT sensors' impedance signatures were slightly changed under the breakage of the center Strand 9. Among sensors (PZTs 1-3, PZTs 5-6, and PZT 8), except for PZTs 4&7 close to damaged Strands 4&7, PZT 1 had the most sensitive variation of impedance responses.

4.2.2 Sensitivity of frequency ranges for strand-breakage monitoring

A sensitive frequency band should be selected for impedance-based strand-breakage monitoring. The RMSD damage metric (Eq. (8)) was utilized to quantify changes in impedance responses induced by the breakage of Strand 4 (PS-2), as shown in Fig. 13. The examined frequency ranges included 9.5-11.0 kHz (Peak 1), 25-28 kHz (Peak 2), and 8-31 kHz (Peaks 1-2). The UCL control threshold was set to make a decision on the occurrence of strand breakage, (see Figs. 13(a)-(c). The RMSD magnitudes were ignorable (less than 1.0%) in the intact case. Due to the damaged strand, the RMSD magnitude of PZT 4 was the most significant (23.2% for Peak 1, 29.1% for Peak 2, and 27.3% for the range 8-31 kHz) and beyond the control threshold. The three frequency ranges had similar sensitivities of impedance responses due to the prestress loss.

4.2.3 Impedance-based monitoring results for three strand-breakage cases

The frequency range 8-31 kHz was selected for strand-breakage monitoring. Fig. 14 shows RMSD indices of PZT1-PZT8 estimated for the three breakage cases (PS-2~PS-4). Error bars were calculated from four ensembles of impedance signatures, as depicted in the figure. The RMSD magnitudes were comparatively small for the intact case (PS-1), and standard deviations of impedance signals were ignorable for the three prestress-loss states (PS-2~PS-4). Thus, it guaranteed low dispersion of the measured data.

Fig. 14(a) shows the impedance monitoring result for the breakage of Strand 4 breakage (PS-2). The RMSD magnitude of PZT 4 had the largest value (27.3%) among the sensors. The local damage was confidently detected as PZT 4 (close to the damaged strand) was beyond the control threshold. The RMSD magnitudes of a few other PZT sensors were also slightly higher than the threshold, thereby indicating variations of prestress forces at other strands.

Fig. 14(b) shows the impedance monitoring result for the breakage of Strands 4 and 7 (PS-3). The RMSD values of PZT 4 (27.8%) and PZT 7 (29.9%) were both significant and higher than the control thresholds. The two damaged Strands 4 and 7 were localized by PZTs 4 and 7 close to them.

Fig. 14(c) shows the impedance monitoring result for the simultaneous damage of Strands 4, 7 and 9 (PS-4). The RMSD magnitudes of all eight PZT sensors were significant and passed the thresholds. The RMSD values of PZT 4 (61.9%) and PZT 7 (56.1%) were dominant among all sensors. It revealed that two outer Strands 4 and 7 were assuredly identified. Moreover, the magnitudes of other PZT sensors were all somewhat significant, in which the third-largest was 35.1% at PZT 1. The result suggests

Table 4 Changes in modal strain energy and prestress-loss estimation under strand breakage cases

Case	Inflicted force*		Modal strain energy change (%)		Relative prestress loss (%)	
	N (kN)	$\frac{dN}{N}$ (%)	$\left(\frac{\delta W}{W}\right)_{1A}$ (Anchorage)	$\left(\frac{\delta W}{W}\right)_{1T}$ (Tube 1)	$\left(\frac{\delta N}{N}\right)_{1A}$ (Anchorage)	$\left(\frac{\delta N}{N}\right)_{1T}$ (Tube 1)
PS-1	266.6	0	0	0	0.00	0.00
PS-2	239.0	10.4	-3.1	-3.1	23.7	23.7
PS-3	211.4	20.7	-4.1	-4.1	31.5	31.5
PS-4	182.5	31.5	-5.2	-7.2	39.3	54.7
PS-5	0	100	-13.2	-13.2	100	100

*The inflicted force in Tube 1 was assumed as a quarter of the total applied force (see Table 3).

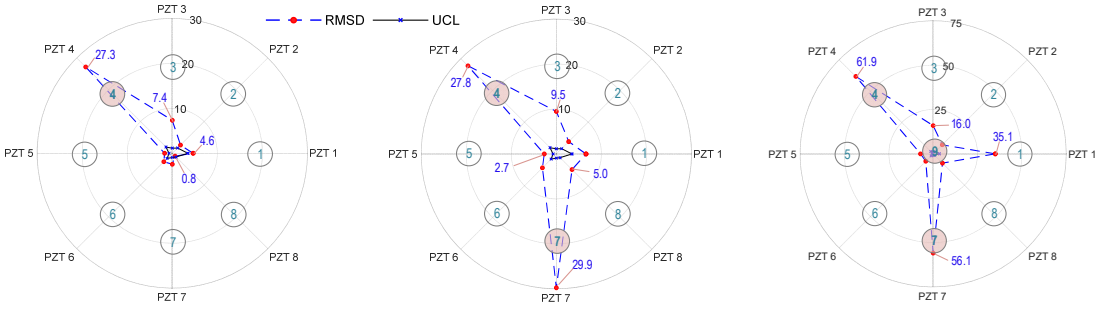

(a) Breakage of Strand 4 (b) Breakage of Strands 4&7 (c) Breakage of Strands 4, 7&9

Fig. 15 Linear tomography of RMSD indices (%) calculated from frequency range 8-31 kHz

damage potentially occurred at the center of Strand 9 or partial damage at other strands.

4.3 Strand-breakage identification by hybrid vibration-impedance monitoring

Global damage estimation in the test structure (i.e., the system of concrete anchorage and tubular frame) was analyzed by modal strain energy change (Eq. (3)). For the four strand-breakage cases (PS-2~PS-5), relative changes in modal strain energies were calculated using changes in natural frequencies. The 1st natural frequency of Tube 1 (see Table 3) was selected for the calculation. As observed in Table 4, modal strain energies of the test structure were gradually reduced by the incremental loss of prestress-forces. The reduced modal strain energy revealed that the structure becomes "softer" under the strand breakage (Nawy 2010).

Local damage detection in the multi-strands anchorage was performed by the linear tomography of RMSD indices (see Eq. (8)). Because the sensitivity of impedance feature (i.e., RSMD index) depends on the distance from a broken strand to measured PZT sensors (Dang *et al.* 2019), the magnitude of RMSD index would be a tomographic indicator for strand-breakage localization. A significant RSMD value and its value beyond the UCL threshold indicate that the strand is potentially damaged. As shown in Figs. 15(a)-(c), RSMD indices and UCL values were plotted on the cross-section of the anchor head for the three breakage cases (PS-2~PS-4) calculated from the frequency range 8-31 kHz with respect to the baseline signal measured at the full-force state (PS-1).

The breakage of Strand 4 (PS-2) caused the prestress-loss of 10.4% of the test structure, relative to the intact prestress force (PS-1), as listed in Table 4. From the vibration-based monitoring, the inflicted structural change was predicted by 3.1% loss of modal strain energy of the 1st vibration mode. The inflicted damage was also predicted by 23.7% loss of prestress-force (using Eq. (4)). The predicted loss was almost equivalent to the failure of two strands, considering the 10.4% of prestress-loss induced by the breakage of a single strand. From the impedance-based monitoring (see Fig. 15(a)), the RMSD value at Strand 4 (27.3%) had the highest and beyond the threshold. The RMSD magnitudes at other strands (e.g., Strand 3) were also beyond the UCL threshold, but those values were not significant as compared to the dominant indication of Strand 4. From the hybrid monitoring, the strand breakage was localized at Strand 4. Moreover, the RMSD tomography suggested that strand breakage causes stress reversal in the anchorage zone.

The breakage of Strands 4 and 7 (PS-3) inflicted the prestress-loss of 20.7% to the test structure (see Table 4). From the vibration-based monitoring, the inflicted structural change was predicted by 4.1% loss of modal strain energy (mode 1). The inflicted damage was also predicted by 31.5% loss of prestress-force. The prediction indicated the failure of about three strands. From the impedance-based monitoring (see Fig. 15(b)), the RMSD indices at Strand 4 (27.8%) and Strand 7 (29.9%) were significantly high and beyond the threshold. Conclusively, the strand breakages were localized at Strands 4 and 7. The RMSD tomography

also indicated stress variations in other strands (e.g., Strand 3 (9.5%) and Strand 8 (5.0%)).

The breakage of Strands 4, 7, and 9 (PS-4) inflicted the prestress-loss of 31.5% to the test structure (see Table 4). From the vibration-based monitoring, the inflicted structural change was predicted by 5.2% loss of modal strain energy (mode 1). The inflicted damage was also predicted by 39.3% loss of prestress-force. The prediction indicated the failure of three or four strands. From the impedance-based monitoring (see Fig. 15(c)), the RMSD magnitudes at Strand 1 (35.1%), Strand 3 (16.0%), Strand 4 (61.9%), and Strand 7 (56.1%) were all significant and beyond the thresholds, thus suggesting multiple damage occurrence. The RMSD magnitudes of Strands 4 and 7 were the first and second most significant and enough to conclude the failure of those strands.

4.4 Discussion on strand-breakage monitoring result

As observed in Figs. 15(b)-(c), the RMSD magnitudes at adjoining strands (e.g., Strand 2) were also beyond the upper control limit UCL, thus indicating the occurrence of minor damage at other strands (with 99.7% confident level). The damage at other strands was originated from stress redistribution in the test structure, and the damage severity was increased for multiple damaged strands. This observation is consistent with the force measured at the right-end strands and previous studies (Abdullah *et al*. 2015(b), Dang *et al*. 2020a). Due to the damage indicator at all strands over the control threshold, it is difficult to identify the accurate number of damaged strands in the triple damage case (in PS-4) with the damage of the center strand. As the global prestress-loss estimation could suggest the number of damaged strands, the combination of hybrid vibration-impedance features yield a better decision on strand-breakage monitoring result.

Overall, the breakage of outer Strands 4 (PS-2) or Strands 4&7 (PS-3 and PS-4) was assuredly identified. However, the breakage of center Strand 9 in the damaged triple strands (PS-4) case was not clearly detected. The number of damaged strands from hybrid vibration-impedance monitoring was somewhat larger than the inflicted one. The following reasons could cause false-positive detection. First, the stress redistribution caused nonlinear changes (e.g., contact stiffness changes) in the test structure. Second, the bonding layer of the PZT interface could be affected by multiple damaged strands. It was reported that the quality of the bonding layer has significant effects on impedance responses (Bhalla and Soh 2004, Yang *et al*. 2008b, Huynh *et al*. 2020). As observed in Table 1, the stiffness of the bonding layer (i.e., E = 5 MPa) was about 40, 14, and 12 times softer than that of the anchorage, interface, and PZT patch, respectively. The bonding-layer effect and the nonlinear distribution of stress-field change along with the anchor-head circumference might cause unequal changes of impedance features, so that the uncertain factors might lead to PZT 1's impedance features being more sensitive to other PZT sensors (e.g., PZT 2) in the damaged triple strands.

5. Conclusions

The hybrid vibration-impedance approach was experimentally assessed for strand-breakage detection in the PSC structure. First, the three-phase framework was designed to alarm damage existence based on changes in vibration characteristics and to localize strand breakage using changes in impedance signatures. Then, the real-scale experiment was conducted on the 9-strand anchorage zone installed on the test structure to measure acceleration and impedance responses under a series of strand-breakage cases. Finally, the experimental results were analyzed to evaluate the practicability of the hybrid-monitoring framework for damage assessment of the test structure.

From the experimental evaluation, the following concluding remarks can be drawn. First, strand breakage caused reductions in the natural frequencies of the PSC structure, which were used to alarm damage occurrence and to estimate relative prestress-force losses. Second, the tomography of RMSD indices can be used to illustrate major damage at local-strand breakage and minor damage induced by stress redistribution in the anchorage zone. Third, the combination of vibration-impedance yielded more accurate locations of damaged strands. The breakage of outer strands in the single and the multiple damage cases were accurately localized, and the center strand breakage in triple damage cases was also localized with some noises.

In general, the hybrid vibration-impedance monitoring scheme practiced here to the lab-scaled anchorage zone of PSC structure can be extended to real-world PSC bridges. Investigation can begin from vibration responses to local impedance characteristics and by crossing information between them. Precisely, vibration responses (e.g., modal frequencies or mode-shapes) can be used to identify abnormalities in dynamic responses and to estimate prestress-loss in tendons. Then, PZT interfaces' impedance features mounted on the anchorages are utilized to determine whether damage existence at the anchorage. Once the damage exists at the anchorage, the RMSD tomography combined with the global prestress-loss estimation is utilized to confirm the locations of strand breakage.

The following work should be taken into account to further investigate the practicability of the proposed framework for damage detection in PSC structures. The prestress-loss model should be improved to consider cable force perturbation and eccentricity due to beam vibration. Also, the effects of environmental changes (e.g., temperature variations) on hybrid vibration-impedance monitoring results need to be analyzed.

Acknowledgments

This work was supported by a grant (21CTAP-C163708-01) from the Technology Advancement Research Program funded by Korea Agency for Infrastructure Technology Advancement (KAIA).

References

Abdulkarem, M., Samsudin, K., Rokhani, F.Z. and A Rasid, M.F. (2019), "Wireless sensor network for structural health monitoring: A contemporary review of technologies, challenges, and future direction", *Struct. Health Monitor.*, **19**(3), 693-735. https://doi.org/10.1177/1475921719854528

Abdullah, A.B.M., Rice, J.A. and Hamilton, H.R. (2015a), "A strain-based wire breakage identification algorithm for unbonded PT tendons", *Smart Struct. Syst., Int. J.*, **16**(3), 415-433. https://doi.org/10.12989/sss.2015.16.3.415

Abdullah, A.B.M., Rice, J.A. and Hamilton, H.R. (2015b), "Wire breakage detection using relative strain variation in unbonded posttensioning anchors", *J. Bridge Eng.*, **20**(1), 1-12. https://doi.org/10.1061/(ASCE)BE.1943-5592.0000639

Ai, D., Luo, H. and Zhu, H. (2019), "Numerical and experimental investigation of flexural performance on pre-stressed concrete structures using electromechanical admittance", *Mech. Syst. Signal Process.*, **128**, 244-265. https://doi.org/10.1016/j.ymssp.2019.03.046

Bhalla, S. and Soh, C.K. (2004), "Electromechanical Impedance Modeling for Adhesively Bonded Piezo-Transducers", *J. Intell. Mater. Syst. Struct.*, **15**(12), 955-972. https://doi.org/10.1177/1045389X04046309

Bonopera, M., Chang, K.C. and Lee, Z.K. (2020), "State-of-the-art review on determining prestress losses in prestressed concrete girders", *Appl. Sci.*, **10**(20), p. 7257. https://doi.org/10.3390/app10207257

Brincker, R., Zhang, L. and Andersen, P. (2001), "Modal identification of output-only systems using frequency domain decomposition", *Smart Mater. Struct.*, **10**(3), p. 441. https://doi.org/10.1088/0964-1726/10/3/303

Cervenka, V. and Ganz, H.R. (2014), "Validation of post-tensioning anchorage zones by laboratory testing and numerical simulation", *Struct. Concrete*, **15**(2), 258-268. https://doi.org/10.1002/suco.201300038

Cho, S., Lynch, J.P., Lee, J.J. and Yun, C.B. (2009), "Development of an automated wireless tension force estimation system for cable-stayed bridges", *J. Intell. Mater. Syst. Struct.*, **21**(3), 361-376. https://doi.org/10.1177/1045389X09350719

Clough, R. and Penzien, J. (1995), *Dynamics of Structures*, (3rd Edition), Computers & Structures, Inc., University Ave, Berkeley, CA, USA.

Dang, N.L., Huynh, T.C. and Kim, J.T. (2019), "Local strand-breakage detection in multi-strand anchorage system using an impedance-based stress monitoring method-feasibility study", *Sensors*, **19**(5), p. 1054. https://doi.org/10.3390/s19051054

Dang, N.L., Huynh, T.C., Pham, Q.Q., Lee, S.Y. and Kim, J.T. (2020a), "Damage-sensitive impedance sensor placement on multi-strand anchorage based on local stress variation analysis", *Struct. Control Health Monitor.*, **27**, p. e2547. https://doi.org/10.1002/stc.2547

Dang, N.L., Pham, Q.Q. and Kim, J.T. (2020b), "Piezoelectric-based hoop-type interface for impedance monitoring of local strand breakage in prestressed multi-strand anchorage", *Struct. Control Health Monitor.*, **28**(1), 1-20. https://doi.org/10.1002/stc.2649

Fang, Z. and Wang, J.Q. (2010), "Practical formula for cable tension estimation by vibration method", *J. Bridge Eng.*, **17**(1), 161-164. https://doi.org/10.1061/(ASCE)BE.1943-5592.0000200

Giurgiutiu, V. and Rogers, C.A. (1998), "Recent advancements in the electromechanical (E/M) impedance method for structural health monitoring and NDE", In: *Smart Structures and Materials 1998: Smart Structures and Integrated Systems*, Vol. 3329, pp. 536-547. https://doi.org/10.1117/12.316923

Gudmundson, P. (1982), "Eigenfrequency changes of structures due to cracks, notches or other geometrical changes", *J. Mech. Phys. Solids*, **30**(5), 339-353. https://doi.org/10.1016/0022-5096(82)90004-7

Hiba, A.J. and Glisic, B. (2018), "Monitoring of long-term prestress losses in prestressed concrete structures using fiber optic sensors", *Struct. Health Monitor.*, **18**(1), 254-269. https://doi.org/10.1177/1475921717751870

Hiba, A.J. and Glisic, B. (2019), "Monitoring of prestressing forces in prestressed concrete structures-An overview", *Struct. Control Health Monitor.*, **26**(8), e2374-1-27. https://doi.org/10.1002/stc.2374

Ho, D.D., Kim, J.T., Stubbs, N. and Park, W.S. (2012), "Prestress-force estimation in PSC girder using modal parameters and system identification", *Adv. Struct. Eng.*, **15**(6), 997-1012. https://doi.org/10.1260/1369-4332.15.6.997

Hoang, T., Fu, Y., Mechitov, K., Sánchez, F.G., Kim, J.R., Zhang, D. and Spencer, B.F. (2020), "Autonomous end-to-end wireless monitoring system for railroad bridges", *Adv. Bridge Eng.*, **1**(1), 1-27. https://doi.org/10.1186/s43251-020-00014-7

Huynh, T.C. and Kim, J.T. (2014), "Impedance-based cable force monitoring in tendon-anchorage using portable PZT-interface technique", *Mathe. Problems Eng.*, **2014**, 1-11. https://doi.org/10.1155/2014/784731

Huynh, T.C. and Kim, J.T. (2017), "Quantitative damage identification in tendon anchorage via PZT interface-based impedance monitoring technique", *Smart Struct. Syst., Int. J.*, **20**(2), 181-195. https://doi.org/10.12989/sss.2017.20.2.181

Huynh, T.C., Nguyen, T.D., Ho, D.D., Dang, N.L. and Kim, J.T. (2020), "Sensor fault diagnosis for impedance monitoring using a piezoelectric-based smart interface technique", *Sensors*, **20**(2), p. 510. https://doi.org/10.3390/s20020510

Kim, J.T. and Stubbs, N. (2003b), "Crack detection in beam-type structures using frequency data", *J. Sound Vib.*, **259**(1), 145-160. https://doi.org/10.1006/jsvi.2002.5132

Kim, J.T., Ryu, Y.S., Cho, H.M. and Stubbs, N. (2003a), "Damage identification in beam-type structures: frequency-based method vs mode-shape-based method", *Eng. Struct.*, **25**(1), 57-67. https://doi.org/10.1016/S0141-0296(02)00118-9

Kim, J.T., Yun, C.B., Ryu, Y.S. and Cho, H.M. (2004), "Identification of prestress-loss in PSC beams using modal information", *Struct. Eng. Mech., Int. J.*, **17**(3_4), 467-482. https://doi.org/10.12989/sem.2004.17.3_4.467

Kim, J.T., Park, J.H., Hong, D.S. and Park, W.S. (2010), "Hybrid health monitoring of prestressed concrete girder bridges by sequential vibration-impedance approaches", *Eng. Struct.*, **32**(1), 115-128. https://doi.org/10.1016/j.engstruct.2009.08.021

Lacidogna, G., Piana, G. and Carpinteri, A. (2019), "Damage monitoring of three-point bending concrete specimens by acoustic emission and resonant frequency analysis", *Eng. Fract. Mech.*, **210**, 203-211. https://doi.org/10.1016/j.engfracmech.2018.06.034

Lacidogna, G., Piana, G., Accornero, F. and Carpinteri, A. (2020), "Multi-technique damage monitoring of concrete beams: acoustic emission, digital image correlation, dynamic identification", *Constr. Build. Mater.*, **242**, p. 118114. https://doi.org/10.1016/j.conbuildmat.2020.118114

Lan, C., Zhou, Z. and Ou, J. (2014), "Monitoring of structural prestress loss in RC beams by inner distributed Brillouin and fiber Bragg grating sensors on a single optical fiber", *Struct. Control Health Monitor.*, **21**(3), 317-330. https://doi.org/10.1002/stc.1563

Lee, S. and Kalos, N. (2014), "Non-destructive testing methods in the US for bridge inspection and maintenance", *KSCE J. Civil Eng.*, **18**(5), 1322-1331. https://doi.org/10.1007/s12205-014-0633-9

Lee, S.Y., Huynh, T.C. and Kim, J.T. (2018), "A practical scheme of vibration monitoring and modal analysis for caisson

breakwater", *Coastal Eng*., **137**, 103-119. https://doi.org/10.1016/j.coastaleng.2018.03.008

Liang, C., Sun, F.P. and Rogers, C.A. (1994), "Coupled electro-mechanical analysis of adaptive material systems-determination of the actuator power consumption and system energy transfer", *J. Intell. Mater. Syst. Struct*., **5**(1), 12-20. https://doi.org/10.1177/1045389X9400500102

Min, J., Yun, C.B. and Hong, J.W. (2016), "An electromechanical impedance-based method for tensile force estimation and damage diagnosis of post-tensioning systems", *Smart Struct. Syst*., *Int. J*., **17**(1), 107-122. https://doi.org/10.12989/sss.2016.17.1.107

Nawy, E.G. (2010), *Prestressed Concrete*: *A Fundamental Approach*, Prentice Hall, Hoboken, NJ, USA.

Nguyen, K.D. and Kim, J.T. (2012), "Smart PZT-interface for wireless impedance-based prestress-loss monitoring in tendon-anchorage connection", *Smart Struct. Syst*., *Int. J*., **9**(6), 489-504. https://doi.org/10.12989/sss.2012.9.6.489

Nie, J.G., Zhou, M., Wang, Y.H., Fan, J.S. and Tao, M.X. (2014), "Cable anchorage system modeling methods for self-anchored suspension bridges with steel box girders", *J. Bridge Eng*., **19**(2), 172-185. https://doi.org/10.1061/(ASCE)BE.1943-5592.0000529

Park, J.-H. (2009), "Development of autonomous smart sensor nodes for hybrid structural health monitoring of large structures", Ph. D. Dissertation; Pukyong National University, Busan, Korea.

Putcha, C., Dutta, S. and Rodriguez, J. (2020), "Risk priority number for bridge failures", *Practice Period. Struct. Des. Constr*., **25**(2), p. 04020010. https://doi.org/10.1061/(ASCE)SC.1943-5576.0000480

Richmond, M., Smolka, U. and Kolios, A. (2020), "Feasibility for damage identification in offshore wind jacket structures through monitoring of global structural dynamics", *Energies*, **13**(21), p. 5791. https://doi.org/10.3390/en13215791

Tadros, M.K., Omaishi, N.A., Seguirant, S.J. and Gallt, J.G. (2003), "Prestress losses in pretensioned high-strength concrete bridge girders", Report No. NCHRP REPORT 496; National Cooperative Highway Research Program, Transportation Research Board, Washington, D.C., USA.

VSL (2018), VSL Strand Post-tensioning Systems, Available online, accessed 12 June 2018. https://vsl.com/home/technologies/post-tensioning-systems/

Wei, F. and Pizhong, Q. (2010), "Vibration-based damage identification methods: a review and comparative study", *Struct. Health Monitor*.: *Int. J*., **10**(1), 83-111. https://doi.org/10.1177/1475921710365419

Yang, Y., Hu, Y. and Lu, Y. (2008a), "Sensitivity of PZT impedance sensors for damage detection of concrete structures", *Sensors*, **8**(1), 327-346. https://doi.org/10.3390/s8010327

Yang, Y., Lim, Y.Y. and Soh, C.K. (2008b), "Practical issues related to the application of the electromechanical impedance technique in the structural health monitoring of civil structures: I. Experiment", *Smart Mater. Struct*., **17**(3), 035008-1-14. https://doi.org/10.1088/0964-1726/17/3/035008

Ye, X., Jin, T. and Yun, C. (2019), "A review on deep learning-based structural health monitoring of civil infrastructures", *Smart Struct. Syst*., *Int. J*., **24**(5), 567-585. https://doi.org/10.12989/sss.2019.24.5.567

Yi, J.-H. and Yun, C.-B. (2004), "Comparative study on modal identification methods using output-only information", *Struct. Eng. Mech*., *Int. J*., **17**(3_4), 445-466. https://doi.org/10.12989/sem.2004.17.3_4.445

Yu, Y., Liu, Y., Chen, J., Jiang, D., Zhuang, Z. and Wu, X. (2021), "Detection method for bolted connection looseness at small angles of timber structures based on deep learning", *Sensors*, **21**(9), p. 3106. https://doi.org/10.3390/s21093106

Zui, H., Shinke, T. and Namita, Y. (1996), "Practical formulas for estimation of cable tension by vibration method", *J. Struct. Eng*., **122**(6), 651-656. https://doi.org/10.1061/(ASCE)0733-9445(1996)122:6(651)

HJ